Journal of Materials Processing Tech. 296 (2021) 117166

Contents lists available at ScienceDirect

Journal of Materials Processing Tech.

journal homepage: www.elsevier.com/locate/jmatprotec

Investigation on solidification structure and temperature field with novel processing of synchronous powder-feeding underwater laser cladding

Yi Liu, Cheng-xin Li *, Xiao-Fang Huang, Hui-Yu Zhang, Chang-jiu Li

State Key Laboratory for Mechanical Behavior of Materials, School of Materials Science and Engineering, Xi'an Jiaotong University, Xi'an, Shaanxi, 710049, China

ARTICLE INFO

Associate Editor: Hui-Ping Wang

Keywords:
Underwater in-situ manufacturing/remanufacturing
Synchronize powder-feeding
Underwater laser cladding
Numerical simulation

ABSTRACT

Synchronous powder-feeding underwater laser cladding(SULC) has a great application prospect in underwater in-situ manufacturing/remanufacturing due to its advantages of small heat input to the substrate and adjustable of additive materials. In this study, the iron-based planar coating with no phase transformation and dilution zone less than 8 μm was prepared on A32 deck steel by SULC using self-designed powder-feeding nozzle and optimizing process parameters. The powder-feeding gas flow rate directly determines the size and stability of the local dry region above the deposition point, and the laser power and powder-feeding rate are the key factors to compensate the laser energy dissipation. Due to the influence of local temperature gradient in SULC, the coating has obvious solidification structure distribution. Columnar grains are mainly distributed upon the trough of fusion line, while dendrites and equiaxed grains are distributed on both sides caused by the temperature gradient becomes smaller and the direction of heat flow changes due to the external environment. In the upper region of SULC coating the equiaxed grains tend to grow up with the increase of laser power. To gain better scientific understanding on differences between atmospheric laser cladding and SULC, the numerical simulation was used to reveal the temperature field changes and coating formation under SULC working parameters. The results show that under the same laser power, due to the forced cooling of larger gas flow and external water environment in SULC process, there is a larger temperature gradient at the deposition point, and the temperature drop rate of the coating and the substrate is greater. In the microstructure, it is shown as columnar grains has a greater directional growth trend. With the increase of laser power, this phenomenon becomes more obvious.

1. Introduction

Underwater additive manufacturing and in-situ repair have great significance for the daily maintenance and emergency repair of ships, energy pipelines and underwater facilities. Moffatt and Thomas (2017) studied in rapid-repair and indicated that rapid-repair concretes are currently used to repair structures such as bridge decks, substructure elements on bridges. High-efficiency underwater additive manufacturing and low-cost in-situ repair techniques have gradually become mainstream and attracted the attention of many researchers. Abbas and Shafiee (2020) suggested that improving the efficiency and effectiveness of maintenance management strategies is imperative.

Seawater as a complex corrosive environment is prone to chemical, electrochemical, and biological corrosion. Submarine facilities are exposed to high-pressure and low-temperature environments for a long time, which makes it more difficult for rapid manufacturing and repair in underwater situations. Song et al. (2004) and Yan et al. (2012) reported effects of the seawater on underwater structure. Gonzalez et al. (2016) and Morita et al. (2006) pointed out that underwater welding and underwater plasma spraying are the two most common techniques of underwater in-situ repair and remanufacturing recently. Underwater plasma spray coatings are even denser than air environment, which can be used to prepare high-performance ceramic coatings as well, but the process parameters are extremely demanding, making it difficult to maintain the repeatability of the process. Joshi et al. (2016) indicated that underwater welding as in-situ repair can be further divided into underwater wet welding and underwater local dry welding. Underwater welding can improve component quality, but moisture and high cooling rates may reduce weld quality, reported by Rowe and Liu (2001). In addition, Wang et al. (2019) also pointed out that high porosity is a serious problem for the melt forming process, and the underwater arc stability of flux-cored wires is difficult to guarantee. Existing underwater in-situ repair and remanufacturing techniques cannot fulfill industrial requirements.

---

* Corresponding author.
E-mail address: licx@mail.xjtu.edu.cn (C.-x. Li).

https://doi.org/10.1016/j.jmatprotec.2021.117166
Received 4 October 2020; Received in revised form 10 March 2021; Accepted 1 April 2021

Laser cladding, which is a kind of planar additive strategy, is widely used in surface repair and remanufacturing in recent years for its wide range of coating selection, small thermal effect on the substrate, and easy to automated production, reported by Cao et al. (2020); Gao et al. (2007); Fiocchi et al. (2020). The introduction of laser additive manufacturing into underwater in-situ repair can effectively take advantage of the laser's high energy density and low coating dilution rate. In recent years, researchers have used wire feeding and preset powder methods for underwater laser cladding studies. Hino et al. (2009) attempted to employ underwater laser cladding technique to the maintenance of radioactive containers and internal components of nuclear power plants through wire feeding and achieved certain results. Feng et al. (2018); (2019) studied the shape controllability of underwater laser cladding 316 L and NAB coatings by the method of preset powder, and the coating was protected by the protective layer and volatile powder. However, these two methods still have limitations in practical applications. The preset powder method is limited by the geometry of the additive component, and at the same time, it increases the operation steps and process difficulty. The wire feeding method requires large heat input, which is easy to cause damage to the heat-sensitive metal substrate.

As the rapid change of temperature during the laser cladding process, it is difficult to figure out the influence law by the experimental method alone, while many researchers research laser cladding through numerical simulation. Seok et al. (2019) presented a methodology to evaluate the local and overall heat transfer characteristics in a short period undergoing the SLM process. Zuo et al. (2019) carried out research on the thermal behavior and grain evolution of 24CrNiMoY alloy steel in laser cladding through a three-dimensional model. Du et al. (2018) studied the thermal behavior of Inconel 625 and its effect on the grain evolution during laser metal deposition. The above researches mainly focus on temperature change by loading heat source on the model in atmosphere. However, the temperature field of laser cladding in special environments, especially the underwater laser cladding has not been studied yet.

Based on the drawbacks of the existing techniques and the advantages of laser cladding, synchronous powder-feeding underwater laser cladding technique(SULC) was studied in this paper. While maintaining metallurgical bonding, the process steps are simplified in SULC as well as the heat input of the laser to the substrate is reduced, and the coating dilution rate is further decreased. The performance was verified by electrochemical analysis. Through the analysis of the grain and phase structure of the coatings, the characteristics of synchronous powder-feeding underwater laser cladding were further explained.

2. Material and method

Arrayago et al. (2019) researched steel used in structural material, A32 deck steel is used for substrate in this experiment for its widely used as a structural material in sea facilities. In this paper, the cladding powder is modified 434 ferritic stainless steel, the compositions are shown in Table 1. The experiment uses a 2.5 kW semiconductor laser with fiber coupled output as the heat source, the shape of laser spot is circular with a Φ2.5 mm focus diameter, the laser beam profile is a Gaussian shaped with the focal length of the laser beam is 199 mm. A homemade nozzle used in SULC method, improved the front-end structure to displace the local water thus promoting the powder aggregation and deposition. The substrate and the front end of the powder-feeding nozzle are completely immersed in water, and the traversing device is controlled by a robot. Fig. 1 shows a schematic diagram of the experiment equipment.

To explore the characteristics of SULC coatings, cross-sectional microstructures were examined by scanning electron microscopy (SEM; MIRA3-LMH; TESCAN, Czech Republic). Metallographic etching of coatings was carried out by using aqua regia solution to highlight the grain structure. Analysis of internal cracks and coatings corrosion resistance by CS310 electrochemical workstation (Corrtest Instruments Co., Ltd, Wuhan, China).

3. Experimental results

3.1. SULC coating macro morphology and performance

Table 2 shows the experimental parameters for the single-pass of SULC, and the single-pass process is instructive to planar structures and can further form three-dimensional additive structures. The parameters different from atmospheric laser cladding reflects unique technical characteristics of SULC and can be shown in the microstructure of the component. In this experiment, Argon was used as the protective gas and the powder-feeding gas. The flow of the protective gas was 1.3m^3/h, the pressure of the powder-feeding gas was 0.4Mpa, and the laser traverse speed was 20 mm/s. Fig. 2 shows the macro photos and cross-section SEM images of single-pass SULC iron-based coating.

The morphology obtained by SULC with the same parameters of laser cladding in atmosphere is shown in Fig. 2(a). Under the same parameters, it was found from the cross-section image that no cladding was formed. Meanwhile, since the poor corrosion resistance of A32 deck steel, the surface is severely oxidized and becomes yellow when the cladding is not formed underwater, cladding did not form under the parameters of (b)(c) neither. The powder-feeding gas flow rate was further improved in(d), (e), (f). It can be seen from the cross-sectional photos that a thin iron-based cladding with a thickness of 20 μm–60 μm is formed on the substrate. Due to the attenuation effect of the underwater environment on the laser and the divergence phenomenon of the powder stream in the water, the thin cladding layer(d–f) has a low dilution rate on the substrate. The basic reason is that the heat input of the laser to the deposition spot is mostly absorbed by the "smoke" formed by water and powder, and fails to form a concentrated heat source. The energy input by the laser into the powder stream decreases, and reduced in the degree of powder melting, which results in a more unidirectional scaly shape on the surface in the underwater single-pass cladding. By increasing the flow of powder feeding gas to reduce the divergence of the powder and the blocking effect of the laser beam by the water environment, a better quality coating is formed as shown in Fig. 2(g)(h). According to the cross-sectional image, the cladding thickness reaches 300 μm–400 μm.

It can be seen from Fig. 2(h) and (i) that further increasing the powder-feeding gas flow rate will not improve the quality of the cladding but the surface of the coating showing a similar morphology to that the flow rate was insufficient. This phenomenon indicating that the powder did not absorb enough heat to melt in these two conditions. Although increasing the gas flow can reduce the local water content, it

Table 1
Composition of A32 substrate and Iron-based powder.

Iron- based powder	C	Cr	Si	Mo	Ni	Mn	Fe
	<0.13	18.96	1.18	0.52	0.94	0.36	——

A32 deck Steel	C	Si	Mn	P	S	Als	Nb	Fe
	0.08~0.13	0.3~0.4	1.0~1.3	≤0.035	≤0.035	≥0.010	0.02~0.04	——

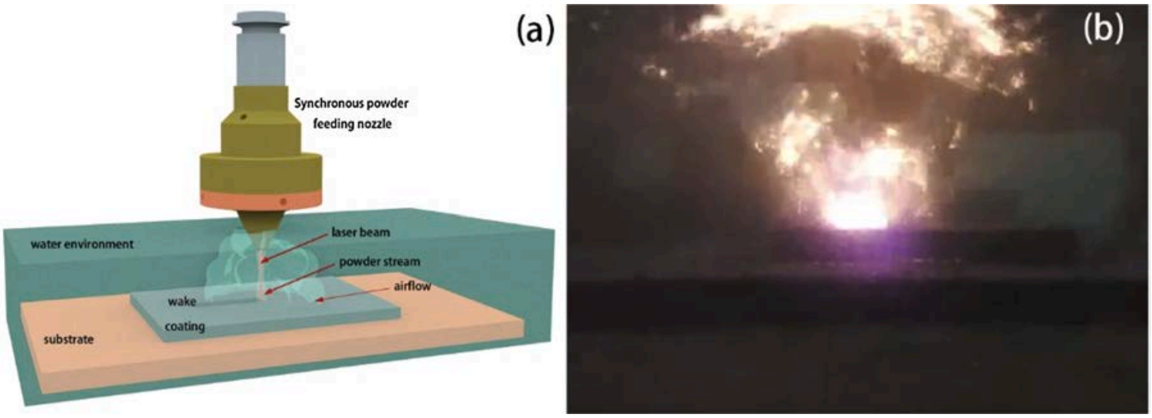

Fig. 1. Schematic and photo of SULC experiment (a)Schematic of experimental equipment(b) photos of synchronous powder-feeding underwater laser cladding experiment.

Table 2
Experimental parameters for single-pass of SULC.

Iron-based	Powder-feeding gas flow rate (L/min)	Laser Power (W)	Powder-feeding rate (g/s)
a	8	1200	0.175
b	8	2000	0.175
c	16	2000	0.175
d	16	2000	0.263
e	20	2000	0.263
f	22	2000	0.263
g	24	2000	0.263
h	26	2000	0.263
i	30	2000	0.263

will seriously affects the continuity of the powder stream and its coupling efficiency with laser beam. At the same time, excessive airflow will cause particles other than the powder convergence point to be drawn into the deposition position, absorbing laser energy and further reducing laser efficiency. Fig. 3 shows the cross-sectional morphology of the single-pass cladding, no penetrating crack but a small amount of non-penetrating microcracks initiate from the surface, shown in Fig. 3 (c), the length is about 60 μm–100 μm. Through subsequent electrochemical tests, the coating still maintains the open circuit potentials (OCP) of the iron-based alloy(Fig. 3(d)) and the corrosion current density is lower than that of the substrate (Fig. 3(e)), proving that no penetrating cracks in the coating that affect the electrochemical performance. Longitudinal cracks are mainly due to the transverse tensile stress generated while the process of solidification. Underwater cladding exhibits tensile stress on the upper layer and compressive stress on the lower layer, which in turn causes the coating to crack. The thermal expansion coefficient of the cladding is close to that of the substrate, and the degree of shrinkage during the solidification process of the two is close, no longitudinal cracks appeared at the bottom of the cladding. A good metallurgical bond is formed between the cladding and the substrate and a clear boundary is observed.

Compared with the single-pass cladding, underwater planar coating

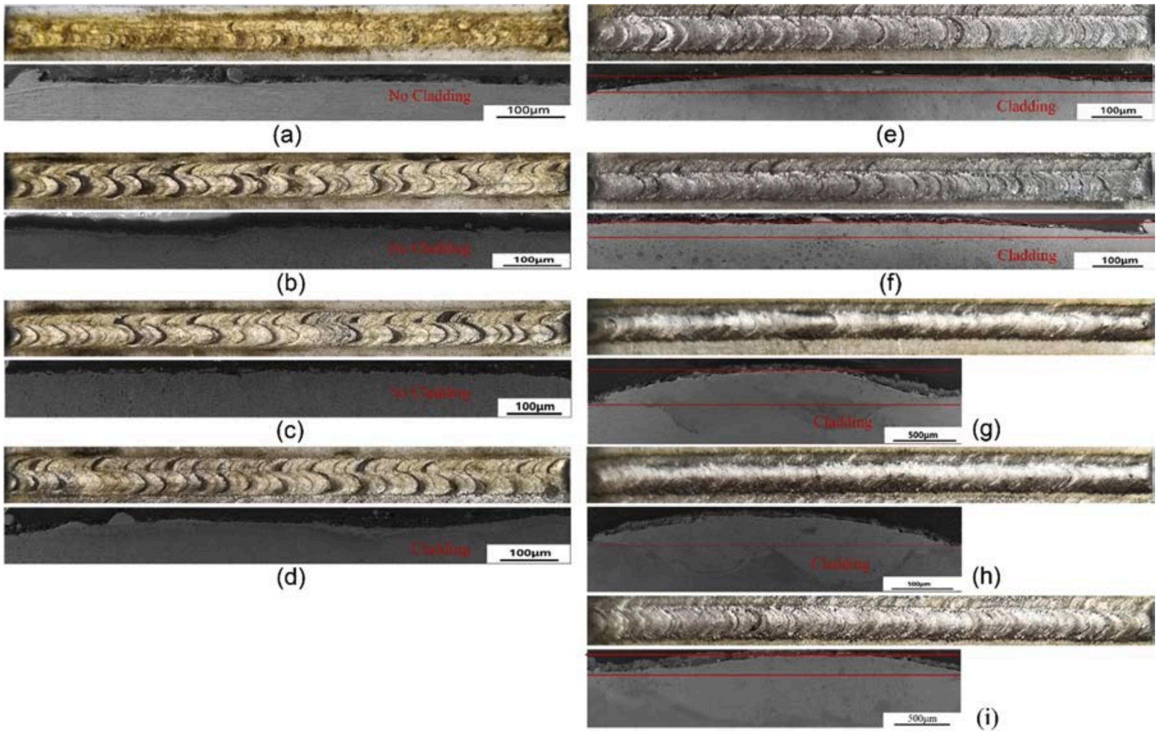

Fig. 2. Macro photos and cross-section SEM images of single-pass SULC iron-based cladding with different parameters (a-i) in Table 2.

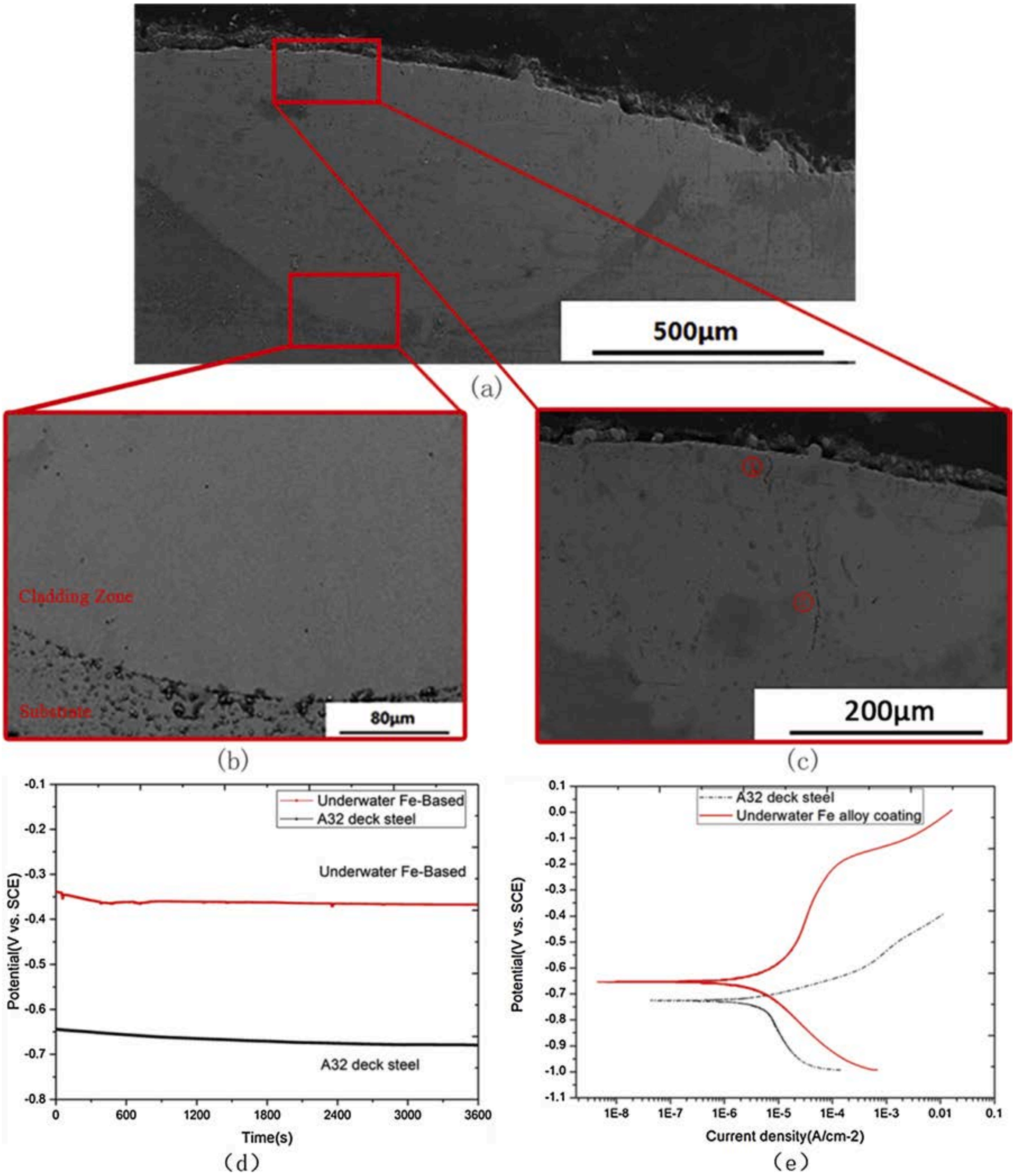

Fig. 3. The cross-sectional morphology of the single-pass cladding(a) macrostructure SEM image (b) bottom region (c) upper region with cracks (d) open-circuit potential (OCP) and (e)polarization curve (PDP) of iron-based coatings.

is subjected to secondary thermal cycling due to the overlap, and the overall structure is more uniform. It can be seen from Fig. 4 that the surface of the underwater planar coating is relatively flat and has obvious overlap marks. Through partial enlargement of Fig. 4(a), a small number of defects parallel to the cladding direction can be found on the surface of the underwater planar coating. These pores are distributed in the overlapping region, which is mainly due to the existence of a small amount of moisture not exhausted by the powder-feeding gas, and the vaporized water on the edge of the high temperature molten pool on both sides of single-pass cladding during the overlap process. By adjusting the overlap rate of the planar coating, the water content at the overlap region can be effectively reduced and the parallel defects can be eliminated. Fig. 4(b) and its partial enlargement show the cross-sectional morphology of the underwater planar coating. The wave-like fusion line produced by the reciprocating motion of the laser beam can be clearly observed. The coating has no obvious cracks, but there is a small number of powders stick on the surface, which is similar to a single-pass cladding. The powder-feeding gas cannot make the last flying particles fall off from the high-temperature surface, make it cannot completely protect the surface.

3.2. Analysis of the forming process of SULC cladding

In the process of atmospheric laser cladding, the laser beam would produce a diffusion radiation transmission mechanism between metal particles, Gusarov and Kruth (2005); Wang et al. (2002) reported this mechanism also exists in SULC process. The gas-liquid two phase flow formed due to the entrainment of the local water by the gas flow

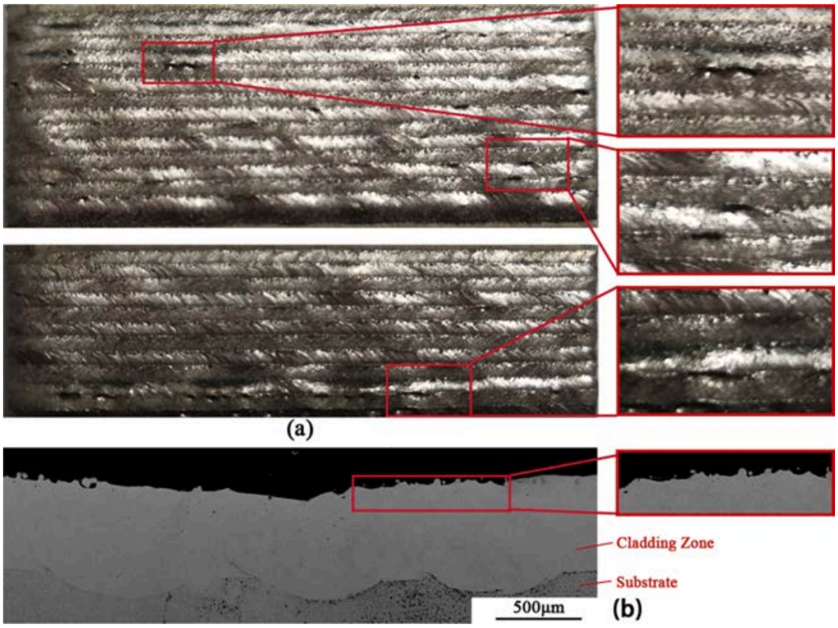

Fig. 4. Planar SULC coating (a)surface overlap morphology and (b)cross-section morphology of underwater coating.

interferes with the powder stream trajectory, and the coupling position between the laser beam and the particles is shifted. The laser energy not only produces diffusion radiation transmission between the deposited particles, but the high-concentration particle smoke further absorbs energy, so that the heat input to substrate and particles is reduced. Ideally, the laser beam only loses a small amount of energy through calm and clean water. As the airflow forms a locally complex multiphase medium around the laser beam, the deviations and energy loss of laser beam will occur. Kwiecień (2018) studied the deflection of laser under the influence of air turbulence, Fu et al. (2020) explained laser intensity attributed to the absorption and scattering of gas molecules and aerosol particles by Beer-Lambert law. These factors can lead to a decrease in coating quality. Based on this, the water content in the multiphase medium above the deposition point can be reduced by increasing the powder-feeding gas flow. Increasing the airflow of the protective gas can avoid the divergence of the powder flow caused by increment of powder-feeding airflow, so that the laser and the powder still meet at the high concentration position of the powder stream. Reducing the working distance of the powder feeding nozzle can also reduce the local water content. At the same time, the number of effective particles can be increased by increasing the powder-feeding rate.

Compared with underwater plasma spraying that requires a stable flame, and underwater cold spraying powered by high-speed airflow, reported by Liu et al. (2020), laser as heat source allows the particle to have more loose deposition conditions. The state of two-phase flow above the deposition point is still extremely affect the melting of particles, and the trajectory of the powder stream is also affected by the two-phase flow. From the above parameters of SULC, continuously increasing the powder feeding gas flow rate to eliminate the water above the deposition point will cause the powder stream disordered, which indicates that there is an optimal parameter between making the multiphase medium turbid and making the powder stream trajectory disordered.

Through the analysis of experimental parameters and coating morphology, the powder-feeding gas flow rate is the most critical factor to ensure a good coupling between the SULC powder stream and the laser beam. The laser power and powder feeding rate are the key factors to compensate for the laser energy dissipation during the deposition, while protecting gas play a role in balancing underwater pressure and improving the quality of underwater coating. Fig. 5 shows the formation process of underwater cladding. Fig. 5(a) is SULC with in-air parameters, since the powder-feeding gas flow rate and the protecting gas flow rate cannot form a local dry region, the multiphase medium above the deposition point is too turbid, continuous coating cannot be formed. Fig. 5(b) is a schematic diagram after increasing the flow rate of protecting gas and powder-feeding gas. Due to the formation of the local dry region, the multiphase medium becomes diluted and coating can be formed. However, the number of particles that can be effectively deposited is reduced for changing gas flow rate, the coating thickness and quality are poor. Fig. 5(c) shows the optimal parameters formed by further increasing the laser power and powder-feeding rate.

3.3. Analysis of SULC coating microstructure

Fig. 6 shows the bottom of the cladding zone(CZ) of single-pass cladding etched with hydrochloric acid and nitric acid at a ratio of 1:3 for 40 s, and its element distribution diagram obtained by energy dispersive spectrometer (EDS). From Fig. 7(a1), it can be seen from the bottom of the CZ that the solidification structure of the cladding has a vertical growth trend. The XRD of iron-based powder, in-air coating and SULC coating is shown in Fig. 6(c). The characteristic peaks of the three materials are basically the same, and the diffraction angles are slightly different due to the difference of the grain size in the coating and the influence of the residual thermal stress, Alam et al. (2019) researched the influence of the residual stress of the coating on the microstructure. The XRD image shows that the SULC coating has no phase transformation. The cladding growth depends on the heat flow gradient in the solidification process. After the powder melted, it solidifies from the upper surface of the substrate, and the local temperature gradient at the bottom of the CZ points to the upper layer of the CZ. The iron-based alloy CZ grows in parallel from the substrate in the opposite direction of the heat flow. When the temperature is stable and the temperature gradient is unchanged, the iron-based alloy grows with columnar grain orientation and gradually appears dendritic morphology. After the temperature gradient is insufficient to maintain the directional growth of the structure or the fractured structure appears in the liquid phase region, dendrites (Fig. 6(a1) yellow dotted) and more equiaxed grain structures (Fig. 6(a2) yellow dotted) appear locally, which is similar to laser cladding in the air.

The thermal affected of the laser on the substrate is the main reason

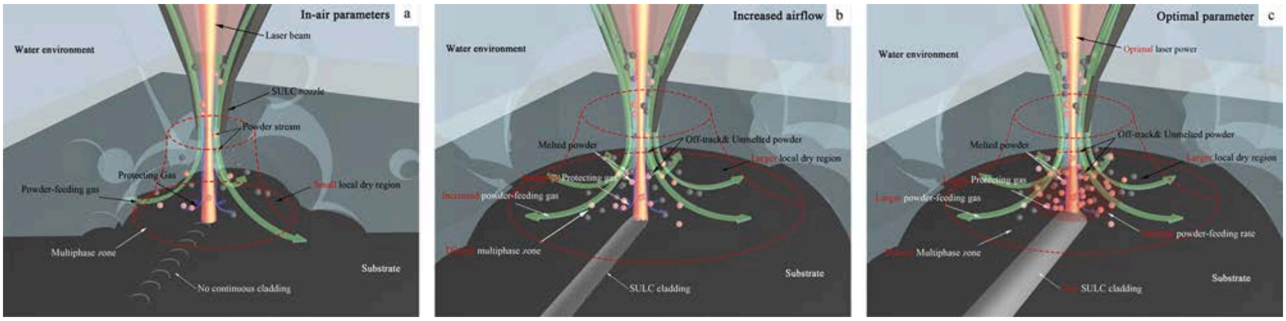

Fig. 5. Schematic diagram of key factors in SULC cladding formation (a) SULC with in-air parameters (b)SULC with increased gas flow rate of powder-feeding gas and protecting gas (c)SULC with optimal parameters.

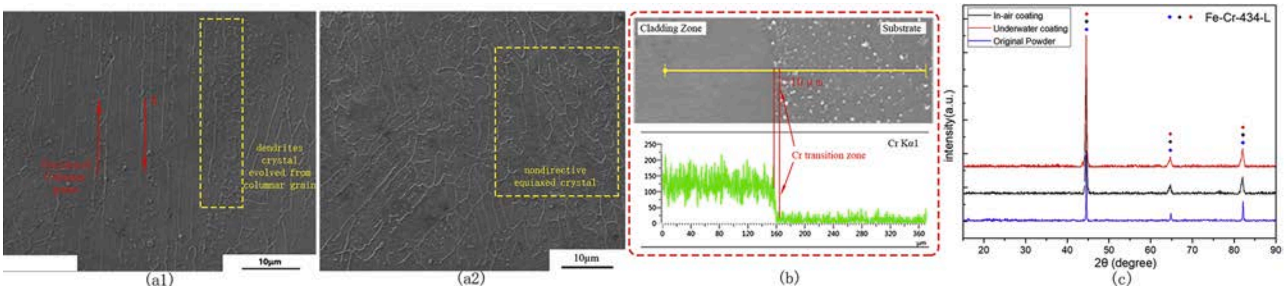

Fig. 6. Bottom morphology of cladding zone (a1)SEM image with columnar grains and dendrites grain (a2) SEM image with nondirective equiaxed grain and(b) element distribution of single-pass underwater cladding (c)XRD pattern of iron-based powder, in-air coating and SULC coating.

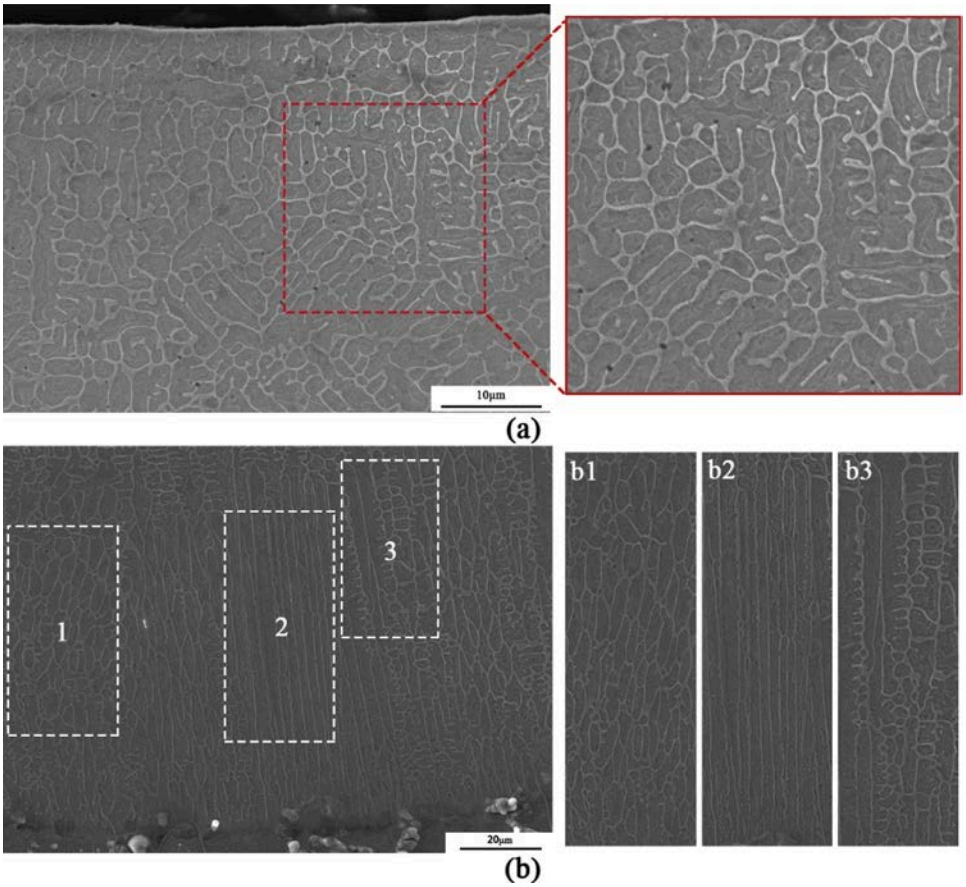

Fig. 7. Etched cross-sectional morphology of underwater planar coating(a) upper region in cladding zone and (b)bottom region in cladding zone with distribution of different grains structure (b1)equiaxed grain region (b2)directional growth of columnar grain region (b3)dendritic structure in the bottom region.

for the elemental dilution of the coating. In SULC process, laser power has been increased, but the forced cooling of the molten pool by the water environment and the blocking of the laser energy by the stronger powder stream caused by the larger powder-feeding gas flow will play a reverse role. The dilution effect of the coating cannot be directly manifested. As the difference of Cr content between the CZ and the substrate is most obvious, the Cr content is used as a calibration for cross-section elemental dilution. The EDS result from Fig. 6(b) shows that the content of Cr element gradually decreases from the CZ to the substrate due to the dilution effect. The thickness of the transition layer in the metallurgical bonding area between CZ and the substrate is less than 8 μm. Compared with the conventional cladding transition layer, the SULC cladding maintains the characteristics of low dilution rate, and the element diffusion is not obvious at the interface.

Fig. 7(a) shows the etched structure of the upper region near the surface of the SULC planar coating cladding zone(CZ). The solidification structure of the upper region of the CZ is mainly affected by the forced cooling of the external water environment and the element segregation in the iron-based alloy. The overall structure is equiaxed grains, which is similar to the upper structure of the atmospheric cladding CZ. Since the grain nucleus temperature is higher than the melt temperature during equiaxed grains growth, it also confirms that the upper melt of CZ has a large degree of undercooling.

Fig. 7(b) is grain growth of bottom region in CZ. From the figure, it can be found that the growth mode of the grains is not uniform, different types of grain can be observed in this region. Fig. 7(b1) is the obvious equiaxed grain region. During the solidification of CZ, no excessive temperature difference between the substrate and the bottom of CZ, and it is difficult to form a surface equiaxed grain region, while the region shown in (b1) is central equiaxed grain evolved from cellular grain. This region usually appears in the upper and middle region of coating. The growth of primary columnar grains is affected by the forced cooling and the multiphase flow formed by the water environment and powder stream during the solidification in SULC process. Branches that fall off the dendrites grow independently, and their solidification heat latent is radially derived from the supercooled liquid to form equiaxed grains region. Fig. 7(b2) shows the directional growth of columnar grain regions at the bottom of the SULC planar cladding zone(CZ). It can be seen from the figure that it has a larger aspect ratio, which is because the grains without dendrite breakage have a greater directional growth trend under a larger temperature gradient and form columnar grains due to the forced cooling effect of water environment. Fig. 7(b3) shows the dendritic structure in the bottom region of the SULC planar CZ. This structure is formed by the gradual transformation to dendrites during the growth of columnar grains.

The solidified structure at the bottom of the cladding zone(CZ) in SULC has different distribution. Fig. 8(a) is a typical region of solidification structure in the fusion line. The unidirectional growth of columnar grains (red dashed frame) is mainly concentrated in the trough of the fusion line. The substrate and coating at this location will absorb more laser energy and be forced to cool down by the external water environment, resulting in a greater temperature gradient. In this region, the grains whose growth direction is antiparallel to the heat flow would grow faster, while the grains of other orientations are eliminated. Compared with atmospheric laser cladding coatings, these columnar grains have a slender structure in the specific direction. It can be seen from Fig. 8(b) that the wave-shaped fusion line produced by the laser overlap of the underwater planar coating. This is because the laser irradiated on each single-pass cladding is partially absorbed by the previous pass, which results in only part of the laser energy being absorbed by the substrate. The grains structure is regularly distributed with the peaks and trough of the fusion line.

In the yellow frame in Fig. 8(a), equiaxed grains and dendrites evolved from columnar grains are mainly distributed, and the overall distribution is shown in the yellow region in Fig. 8(b), which is located on both sides of the columnar grain in the trough of the fusion line. The temperature gradient is relatively gently in this region. In addition, since the solidification direction at this region is not completely parallel to the direction of heat flow, gravity and Marangoni effect are more obvious during the solidification process, (Reuther et al., 2019; Kühn G., et al. 1984) researched flow behavior in molten pool due to temperature field. It is easier to break when the grains grow, and produce new fine-nucleus, which form equiaxed grains in uniform directions.

4. Discussion

4.1. Comparison between coatings of SULC and atmospheric laser cladding

Fig. 9(a) is a macroscopic comparison photo of the single-pass atmospheric laser cladding coating and SULC coating prepared with the same experimental parameters (the optimal parameters in atmosphere). Using the same powder feeding gas flow as the atmospheric laser cladding is not enough to make the powder in the SULC process form a continuous coupling state with laser beam, and the powder cannot absorb the laser energy to melt and fly to the substrate for solidification.

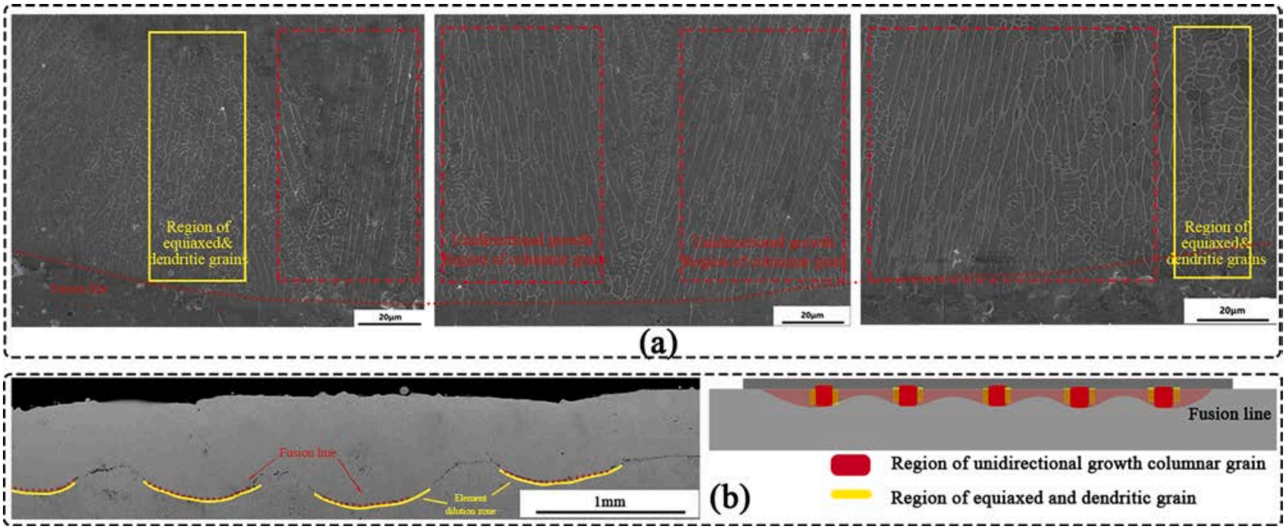

Fig. 8. Grain growth mode distribution of underwater planar coating(a) different region with different grain structure (b) macrostructure image and schematic of grains structure distribution.

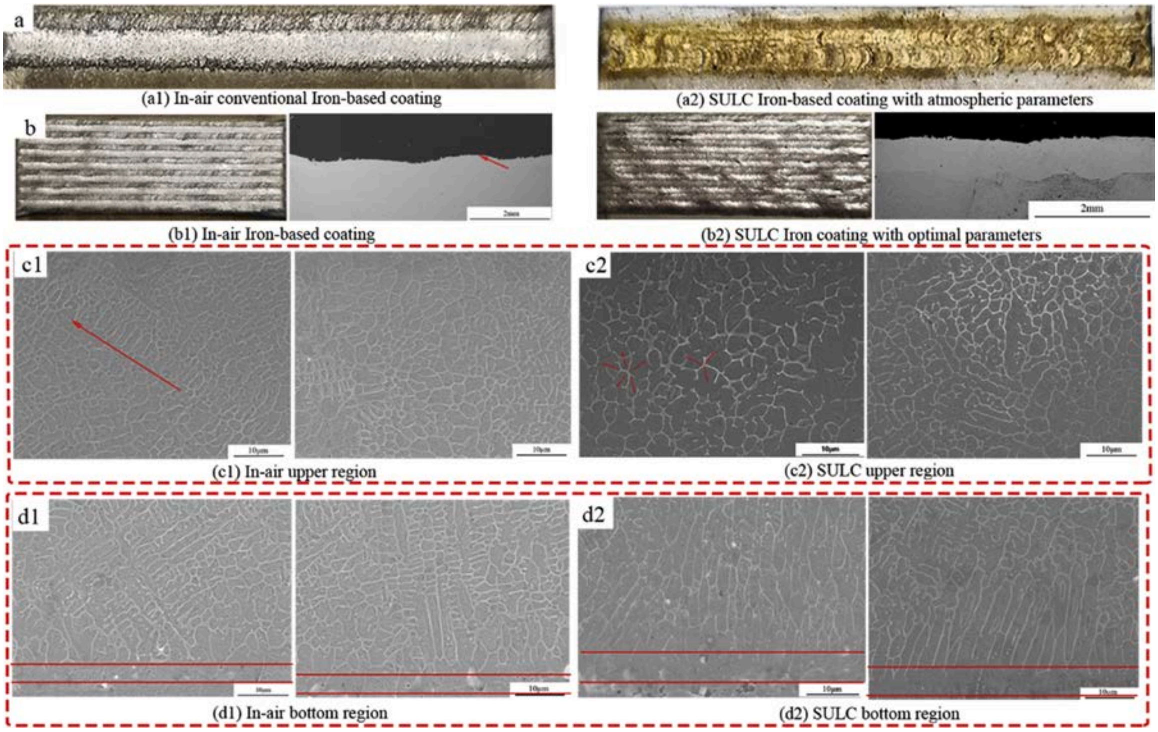

(a1) In-air conventional Iron-based coating

(a2) SULC Iron-based coating with atmospheric parameters

(b1) In-air Iron-based coating

(b2) SULC Iron coating with optimal parameters

(c1) In-air upper region

(c2) SULC upper region

(d1) In-air bottom region

(d2) SULC bottom region

Fig. 9. Comparison of iron-based coating in two methods (a)atmospheric and SULC laser cladding under the same parameters (b)macrostructure and SEM image of two kinds of coatings (c)upper part of two kinds of planar coatings (d)bottom of two kinds of planar coatings.

At the same time, the protecting gas in SULC cannot make the surface of the coating protected due to the external water pressure, which further increases the formation conditions of the SULC coating, resulting no continuous coating formed in atmospheric parameters. As mentioned earlier, simply increasing the powder feeding gas flow rate can remarkable improves the quality of the coating within a certain range, but the best coating cannot be obtained. The best underwater coating can be obtained by increasing the laser power and the powder feeding speed together. This shows that the most important factors in the SULC process are to maintain the complete trajectory of the powder stream and maintain a good coupling with the laser beam.

Fig. 9(c) is the SEM images of the etched coating at the upper part of CZ by two methods. In the cross-sectional image of the atmospheric coating(c1), the residual dendrite branches that grow obliquely upward can be observed. Combined with the location of(b1), it is deduced that which is due to the solidification of cellular dendrite being disturbed and the solute segregation. The grain of CZ solidifies in the direction of heat flow. Mainly structure in the upper part of the atmospheric cladding CZ is non-oriented equiaxed grains formed due to solute segregation and supercooling. (c2) is cross-sectional image of the upper part of the SULC cladding zone(CZ), the microstructure is biased towards equiaxed grains, and there is no obvious cellular grain morphology related to the heat flow. Equiaxed grains are grown using supercooled melt as a heat sink, and the equiaxed grains in the alloy are affected by melt convection and solute segregation. From the second images of(c1) and (c2), the grain size of upper region in the SULC coating is larger than that of conventional laser cladding, which is combined effect of the larger laser power causing the grain to grow and the forced cooling of the upper surface with the water environment produces a larger temperature gradient to inhibit the grains growth.

The bottom of cladding zone with two methods are shown in Fig. 9 (d). The two kinds of coatings have a lower solute enrichment at the interface, a larger temperature gradient, and smaller crystallization rate, which is conducive to the growth of planar grains. The planar grain width of the underwater cladding is larger than that of the conventional cladding, which may be because the temperature gradient at the interface of the underwater cladding is larger and the composition has a lower degree of undercooling, which is more conducive to the growth of planar grains. The growth width of the planar grains does not represent the dilution of the elements. Due to the low solute enrichment and the large temperature gradient at the bottom of the SULC coating, the dilution zone does not increase significantly when the laser power increases.

The microhardness as a mechanical property can directly reflect the microstructure. Fig. 10 shows the hardness of the coating prepared by the two methods. As shown in the figure, the hardness of the coating prepared by the SULC in the heat-affected zone of the substrate is slightly higher than that of the same iron-based coating prepared in conventional laser cladding. This may be due to the forced cooling of the SULC by the water environment and large gas flow, resulting in a smaller dilution zone near the interface, which is verified in subsequent simulation results. Above the interface, the hardness of the SULC coating is close to the original iron-based powder, and slightly lower than in-air

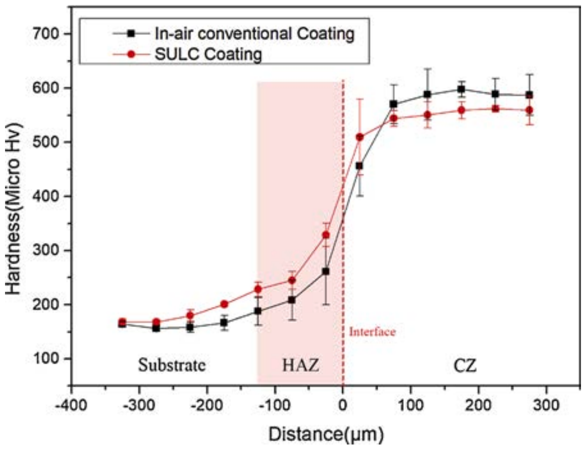

Fig. 10. Microhardness of the coating prepared by the two methods.

coating. Through the comparison of Fig. 9, this is because larger columnar grains in the bottom region caused by larger heat flow gradient and larger equiaxed grains in upper region formed by the higher laser power, which makes the hardness at this position lower.

4.2. Numerical simulation results

To further explore the reasons for the difference in the coating structure between the two methods, the temperature field of laser cladding in different external environments was simulated by finite element numerical simulation. Song et al. (2021) and Geng et al. (2020) researched heat transfer and solidification morphology of molten pool in laser cladding and laser welds. Considering that SULC is an additive process, a three-dimensional model coupling *heat transfer in solid and fluid* and *solid mechanics* modules was used in the COMSOL software (Version 5.4 COMSOL Inc.) by using explicit transient methodology. The heating effect of the laser on the substrate is simulated by an equivalent heat source. Different external environmental convection heat transfer coefficients correspond to different external environmental medium. A node activation model is utilized to simulate the formation of the coating, melting temperature as a criterion to activate the node.

The model shown in Fig. 11(a) described the generation of iron-based coating under laser heat source with and without water environment. Only 1/2 of the entire model was solved by using symmetry conditions for saving memory of computer so that simulations of coupling multiphysics could be performed in the future. The substrate domain used free tetrahedral mesh, the activation domain used a hexahedral mesh and the mesh is encrypted at the heat source concentration location to improve calculation convergence and save calculation space, as shown in Fig.11(a2). Because of the traverse speed is 20 mm/s, Tamanna et al. (2019) explained the Gaussian model can better reflect the heat effect than the double ellipsoidal model, as shown in Eq.1. Wei et al. (2016) and Li et al. (2020) discussed the shape and heat flow distribution of the melting pool by means of the heat transfer mode in the laser cladding process using the two-dimensional model and the section of three-dimensional model. In the model, natural convection is used on the vertical wall and bottom of the calculation domain, and forced convection of water is adopted on the top surface while forced convection of Ar is adopted on the surface of activation region due to the forced airflow of powder-feeding gas. as shown in Fig. 11(a1) and Eqs. 2–4.

$$-\boldsymbol{n}\cdot\boldsymbol{q} = Q_b = (1-\varepsilon)\left(\frac{3\cdot p_{laser}}{pi\cdot {r_{spot}}^2}\right)\cdot e^{\frac{-2\cdot r\_focus^2}{r\_spot^2}} \tag{1}$$

Where ε is surface emissivity of substrate and additive material, p_{laser} is laser power of equivalent heat source, r_{spot} is the radius of laser spot and *r_focus* is distance to the center of the heat source. The heat flux from the equivalent heat source to the surface is Q_b.

$$Q_0 = h\cdot(T_{ext}-T)h = \frac{k}{L}\left(0.68+\frac{0.67\cdot {R_e}^{1/4}}{\left(1+\left(\frac{0.492\cdot k}{\mu\cdot C_p}\right)^{9/16}\right)^{4/9}}\right) \tag{2}$$

$$Q_1 = h\cdot(T_{ext}-T)h = \frac{k}{L}0.54Re_L^{1/4} \tag{3}$$

$$Q_2 = h\cdot(T_{ext}-T)h = \frac{2k}{L}\cdot\frac{0.3387{P_r}^{1/3}Re_L^{1/2}}{\left(1+\left(\frac{0.0468}{P_r}\right)^{2/3}\right)^{1/4}} \tag{4}$$

Where T_{ext} is external temperature, k is heat transfer coefficient, L is characteristic length and P_r is the Prandtl criterion.

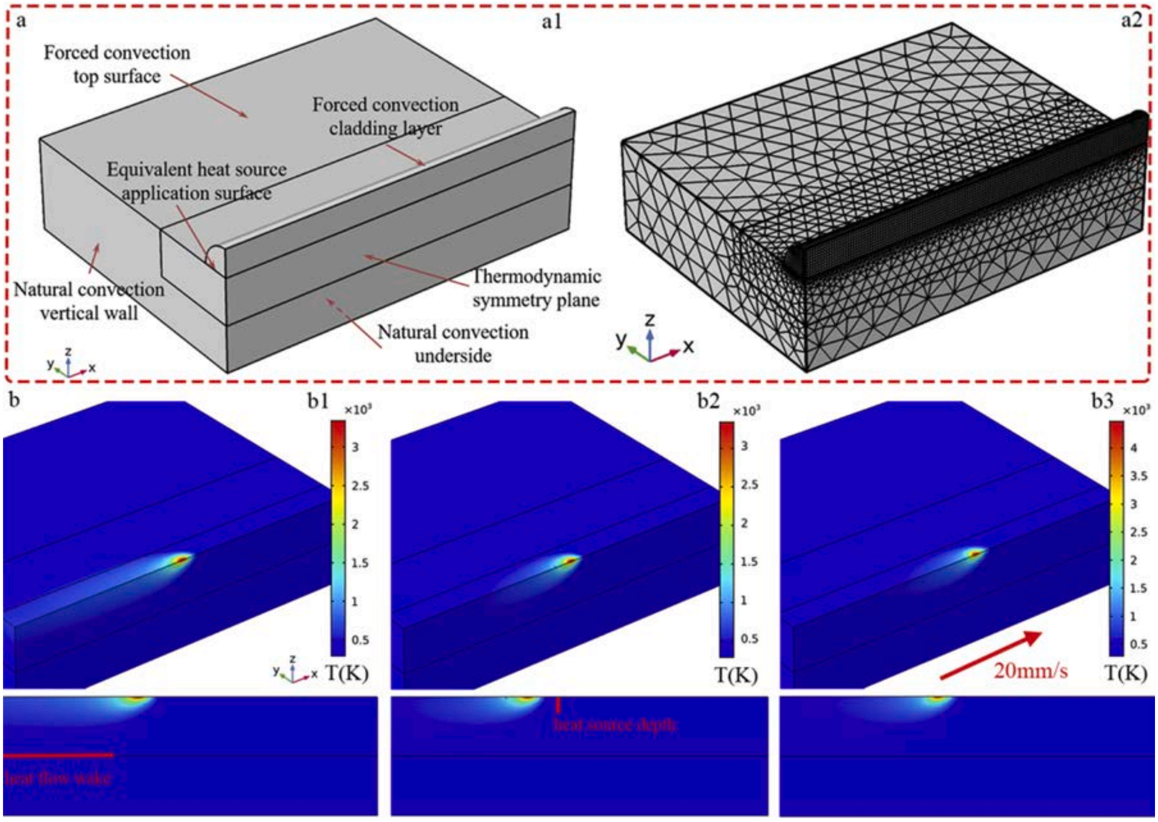

Fig. 11. Numerical simulation model of SULC (a1) geometric model and (a2) mesh of calculation domain and temperature field without cladding domain in water and atmospheric environment (b1)1200 W atmospheric laser cladding (b2) 1200 W SULC (b3) 1600 W SULC.

Fig.11(b) shows the temperature field of underwater laser cladding and atmospheric laser cladding without cladding material domain. From the temperature field, it can be found that as the low traverse speed of the heat source, the heat is mainly concentrated in the center spot of the equivalent heat source, however, compared with the temperature field after introducing water environment heat exchange in (b2) and (b3), (b1) has a more obvious heat source wake. The wake of the heat source indicates that there is higher heat accumulates in the substrate, and it is difficult for the heat to be dissipated in a short time after the heat source leaves. Under the same laser power of 1200 W, the temperature of the center spot of two processes is very close, and the underwater cladding is slightly lower than that in atmosphere. Affected by the forced convection of the water environment on the top surface of the calculation domain and the natural convection on the vertical wall, the temperature rise region more concentrated, and the heat dissipation is faster, which could be easier find in the cross-section of the temperature field. As shown above in Fig.8, it is easier to observe columnar grains with obvious growth trend near the substrate of SULC, which is consistent with the simulation results of a more concentrated and larger local gradient temperature field.

Due to the difference between synchronous powder-feeding laser cladding and powder bed laser sintering, the equivalent heat source is applied between the coating and the substrate instead the surface. The temperature field of the substrate in Fig.11(b) shows heat dissipation and the depth of the heat source, while the temperature of the cladding calculation domain could directly shows the surface heat dissipation of the cladding formation and deposition process in Fig. 12. Fig. 12(a) is isotherm diagram of 1200 W atmospheric cladding, Fig. 12(b) (c) are underwater cladding isotherm diagram with 1200 W and 1600 W. The thermal distribution of SULC is more concentrated at the deposition point. With the increase of laser power, the wakes of coating and substrate tend to be shorter, which indicates that the cooling rate of SULC is more obvious with the increase of laser power. From the cross-section in Fig.12(b)(c), the temperature distribution is extremely uneven in substrate and cladding calculation domain, the heat dissipation in the cladding zone is faster than substrate, and the macro behavior is that the cladding has a higher cooling rate because of the forced convection on the top surface by larger gas flow and multiphase flow containing water. Corresponding to the results of numerical simulation, it is difficult to keep enough temperature gradient during atmospheric laser cladding and form stable columnar grains near the substrate, grains tend to grow laterally into dendrites, as shown in Fig.12(d). With the increase of laser power, the local temperature gradient becomes larger and the columnar grains becomes slender in (e)(f). Fig.12(g) is the typical grain growth of the coating in atmospheric laser cladding near surface and (h)(i) are SULC cladding grain growth near surface with laser power increasing. In

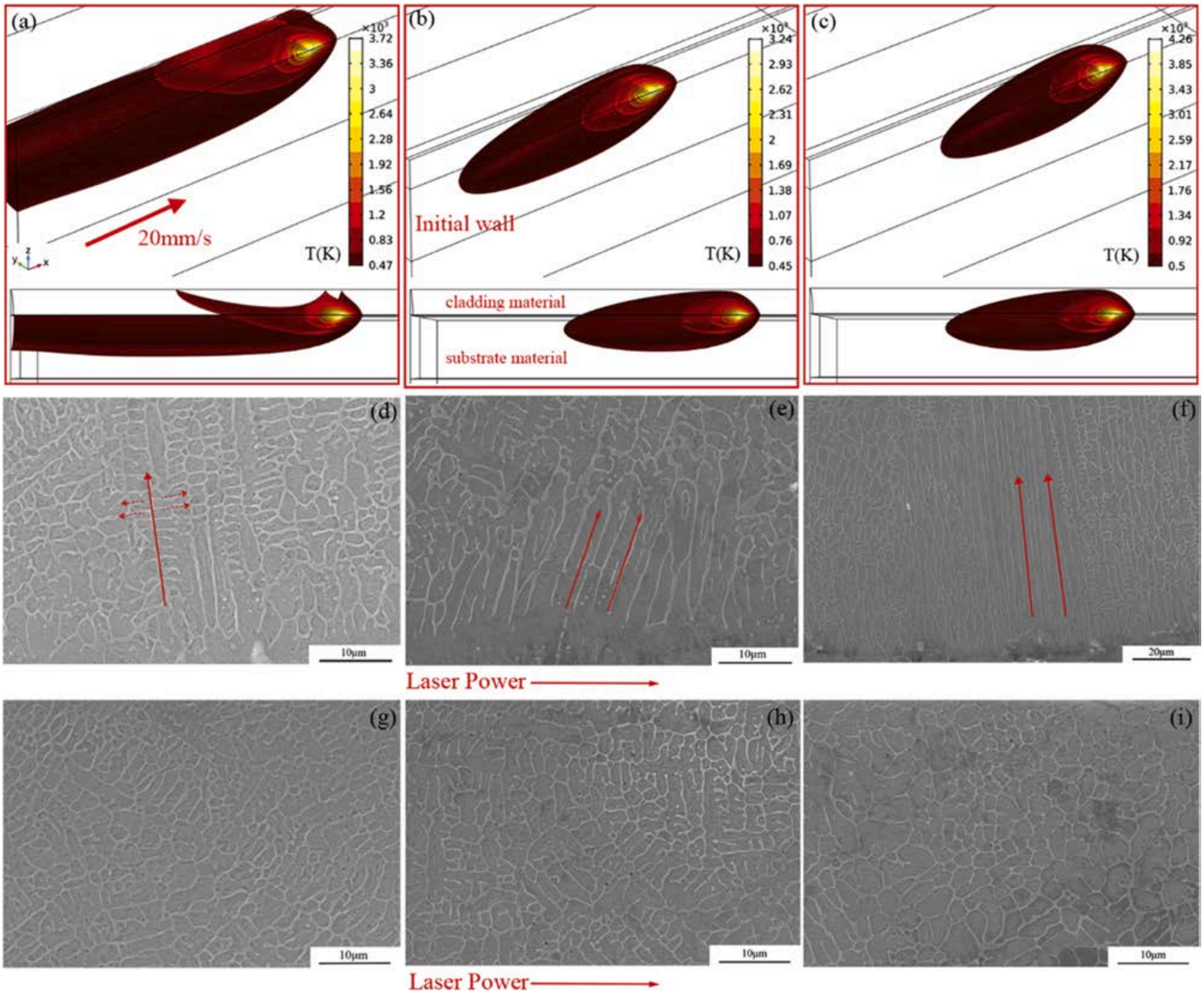

Fig. 12. Isotherm diagrams and typical grain growth modes in SULC and in-air laser cladding (a)atmospheric 1200 W (b) SULC 1200 W (c) SULC 1600 W. (d) atmospheric cladding grain growth near substrate (e-f) SULC cladding grain growth near substrate with laser power increasing (g) atmospheric cladding grain growth near surface (h-i) SULC cladding grain growth near surface.

the upper part of the coating, equiaxial grains are dominant in both methods. However, the grain size of SULC coating increases with the increase of laser power.

Activating nodes through temperature criterion could qualitatively judge the generation of cladding and simulate the process of cladding formation. Fig. 13(a)(b)(c) show the mesh activation results at in-air 1200 W, underwater 1200 W, and underwater 1600 W, respectively. The graphs of the change of the nodes temperature with time corresponding to the (0, 0, Z) coordinates are shown below. Comparing the mesh activation cloud diagram, it is found that atmospheric cladding has the most activated nodes, that is, most nodes reach the temperature threshold. With the laser power increasing in underwater cladding, more nodes are activated. The experimental results corresponding to the simulation results are given under the cross-section of mesh activation cloud diagram, and the experimental results are the same as the simulation trend. Under the same laser power, the thickness of SULC coating is lower than that of in-air conventional laser cladding. With the increase of laser power, the thickness of SULC coating increases. This is mainly due to the forced cooling of the upper surface of the cladding by gas flow and multiphase flow during SULC process. Only a small amount of powder can absorb enough energy to form the coating. With the increase of laser power, the energy loss caused by forced cooling is further compensated, so that the thickness of the coating increases. The nodes in the ellipse circle are the nodes that are activated, which is consistent with the cloud diagram and the experiment. The cooling curve after the first temperature rise corresponds to the smaller temperature wake of underwater cladding in Fig. 11(b), proving a higher cooling rate in SULC.

4.3. Model of SULC coating solidification mechanism

The solidification structure of the SULC coating is consistent with the calculation simulation of temperature field and conforms to the solidification law. Tan et al. (2020) studied the microstructure of titanium alloy by laser-solid-formed-produced, which provided a reference for the study of laser cladding solidification structure. The model of iron-based SULC coating solidification mechanism in water environment can be basically summarized as Fig. 14.

Due to the influence of the water environment containing powder and gas above the deposition point, while increasing the laser power and powder feeding rate to form a good quality coating. The substrate absorbs more laser energy and forms a more obvious fusion line at the interface, the numerical simulation results show that the maximum temperature of the substrate and coating under the optimal parameters of SULC is higher than that of the in-air conventional laser cladding. However, the diffusion of elements in the coating to the substrate is still controlled within 8 μm. Since the solidification process of the SULC coating starts after laser irradiation, the slope of the local melting point curve at the front of the solid-liquid interface is greater than the slope of the actual temperature distribution curve, and the temperature gradient is used as the driving force to solidify, forming an unstable interface.

It can be seen from the Fig. 14 that the large temperature gradient

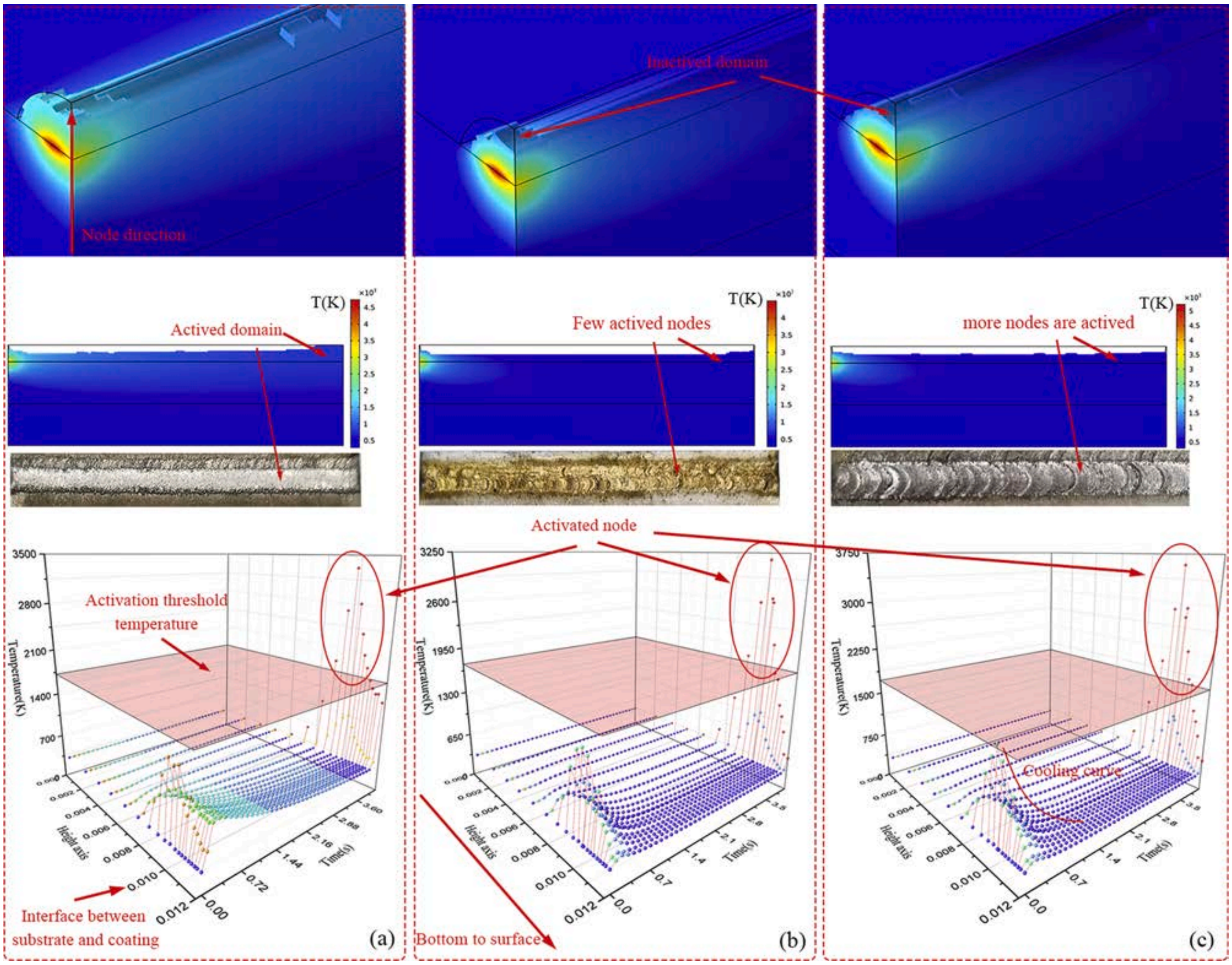

Fig. 13. Simulation and experimental results of activation domain and change of the nodes temperature with two cladding methods (a) atmospheric 1200 W (b) SULC 1200 W (c)SULC 1600 W.

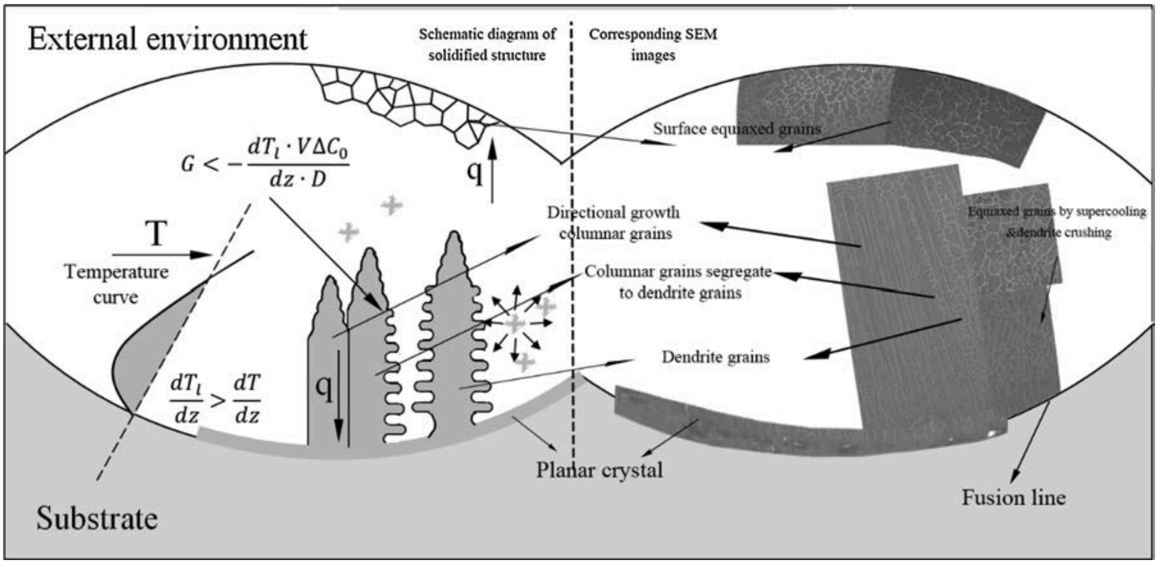

Fig. 14. Schematic diagram of heat flow change and solidification structure distribution in SULC cladding.

and low solute enrichment caused by the water environment in the initial stage of solidification make the coating have a greater tendency to grow planar grains. At the bottom of the coating, the forced directional growth of dendrites grains is concentrated in the trough of the fusion line. The columnar grains are formed by preferential orientation in the anti-parallel direction of heat flow, which grows perpendicular to the fusion line, Fu et al. (2021) showed similar phenomenon in underwater in-situ wire-feeding laser cladding 304 stainless steel. The temperature gradient in the underwater environment promotes a more significant growth trend in the direction of the primary dendrite, and the growth of columnar grains is narrower than that in atmospheric coating. Combined with the isotherm diagrams in Fig. 12, this is mainly due to the changes in the thermodynamic coefficients caused by the SULC process parameters and the underwater environment, thereby forming a locally larger temperature gradient. With the growth of the columnar grains, the area of constitutional supercooling will gradually decrease, and the supercooling exists at the tip of the primary dendrite to form the dendritic structure. In the growth process of the directionally grown columnar grains, the branches shed from the dendrites and grow independently, forming equiaxed grains on both sides. The middle and upper part of the cladding is mainly the central equiaxed grain, since the increase in laser power, the grains in upper region are slightly larger than in-air conventional laser cladding. Using the growth form of the solidified structure, a coating with a specific structure can be obtained.

5. Conclusion

In this study, the synchronous powder-feeding underwater laser cladding(SULC) iron-based coating with a uniform structure and fine quality was prepared, and the influence of water environment on laser cladding was analyzed by solidification structure and numerical simulation. The main conclusions are as follows:

1) By optimizing the structure of the powder-feeding nozzle and adjusting the process parameters, the iron-based coating with a thickness of more than 500 μm can be deposited on A32 steel by synchronous powder-feeding underwater laser cladding(SULC).
2) The powder-feeding gas flow rate, laser power and powder-feeding rate are the key factors to determine the deposition and quality of SULC coating. The powder-feeding gas flow rate directly determines the size and stability of the local dry region above the deposition point, and the laser power and powder-feeding rate are the key factors to compensate the laser energy dissipation.
3) Under the optimal parameters, the dilution zone of SULC coating is less than 8 μm, there is no through cracks and the corrosion current density of the coating is lower than that of the substrate. The microhardness of SULC coating is about 550Hv, slightly lower than that of atmospheric coating due to the increase of laser power and larger grains.
4) Due to the influence of local temperature gradient in SULC, columnar grains are mainly distributed upon the trough of fusion line, and the equiaxed grains in the upper region of SULC coating tend to grow up with the increase of laser power. By further adjusting the parameters, the functional coating with more uniform solidification structure can be obtained.
5) The numerical simulation results show that under the same laser power, due to the forced cooling of larger gas flow and external water environment in SULC process, there is a larger temperature gradient at the deposition point, and the temperature drop rate of the coating and the substrate is greater. In the microstructure, it is shown as columnar grains has a greater directional growth trend. With the increase of laser power, this phenomenon becomes more obvious.

Although the interaction between laser and powder in the multiphase medium of water environment in synchronous powder-feeding underwater laser cladding needs to be studied, it will be widely used in the field of marine repair or the preparation of special solidified structure coating in the future due to its small heat input and large material adjustability.

CRediT authorship contribution statement

Yi Liu: Conceptualization, Software, Investigation, Writing - original draft, Writing - review & editing. **Cheng-xin Li:** Conceptualization, Supervision, Funding acquisition. **Xiao-Fang Huang:** Investigation. **Hui-Yu Zhang:** Visualization. **Chang-jiu Li:** Conceptualization, Supervision.

Declaration of Competing Interest

The authors declared no conflict of interest.

Acknowledgements

This work was financially supported by the National Key Research and Development Project (No. 2018YFB2002000), Key Technology

Research and Development Program of Shandong (No. 2019JZZY010802), National Natural Science Foundation of China (No. 51761145108), all of the authors are grateful to the financial support.

References

Abbas, M., Shafiee, M., 2020. An overview of maintenance management strategies for corroded steel structures in extreme marine environments. Mar. Struct. 71 (December 2019), 102718 https://doi.org/10.1016/j.marstruc.2020.102718.

Alam, Mohammad K., Edrisy, Afsaneh, Urbanic, Jill, 2019. Microstructural analysis of the laser-cladded AISI 420 martensitic stainless steel. Springer US 50 (5). https://link.springer.com/article/10.1007/s11661-019-05156-6.

Arrayago, I., Real, E., Mirambell, E., Marimon, F., Ferrer, M., 2019. Experimental study on ferritic stainless steel trapezoidal decks for composite slabs in construction stage. Thin Walled Struct. 134 (September 2018), 255–267. https://doi.org/10.1016/j.tws.2018.10.012.

Cao, Q., Bai, Y., Zhang, J., Shi, Z., Ying, J., Fu, H., Wang, H., 2020. Removability of 316L stainless steel cone and block support structures fabricated by Selective Laser Melting (SLM). Mater. Des. 191, 108691 https://doi.org/10.1016/j.matdes.2020.108691.

Du, L., Gu, D., Dai, D., Shi, Q., Ma, C., Xia, M., 2018. Relation of thermal behavior and microstructure evolution during multi-track laser melting deposition of Ni-based material. Opt. Laser Technol. 108, 207–217. https://doi.org/10.1016/j.optlastec.2018.06.042.

Feng, X., Cui, X., Jin, G., Zheng, W., Cai, Z., Wen, X., Liu, J., 2018. Underwater laser cladding in full wet surroundings for fabrication of nickel aluminum bronze coatings. Surf. Coat. Technol. 333 (November 2017), 104–114. https://doi.org/10.1016/j.surfcoat.2017.10.056.

Feng, X., Cui, X., Zheng, W., Wen, X., Zhao, Y., Jin, G., et al., 2019. Performance of underwater laser cladded nickel aluminum bronze by applying zinc protective layer and titanium additives. J. Mater. Process. Technol. 266 (October 2018), 544–550. https://doi.org/10.1016/j.jmatprotec.2018.11.036.

Fiocchi, J., Bif, C.A., Tuissi, A., 2020. Selective laser melting of high-strength primary AlSi9Cu3 alloy: processability microstructure and mechanical properties. Mater. Des. 191. https://doi.org/10.1016/j.matdes.2020.108581.

Fu, Yunlong, Guo, Ning, Li, Zhou, Qi, Cheng, Jicai, Feng, 2020. Underwater wire-feed laser deposition of the Ti-6Al-4V titanium alloy. Mater. Des. 186 (C) https://doi.org/10.1016/j.matdes.2019.108284.

Fu, Yunlong, Guo, Ning, Cheng, Zhou, Guanghui, Wang, Jicai, Feng, 2021. Investigation on in-situ laser cladding coating of the 304 stainless steel in water environment. J. Mater. Process. Technol. 289. https://doi.org/10.1016/j.jmatprotec.2020.116949.

Gao, Y.L., Wang, C.S., Yao, M., Liu, H.B., 2007. The resistance to wear and corrosion of laser-cladding Al2O3 ceramic coating on Mg alloy. Appl. Surf. Sci. 253 (12), 5306–5311. https://doi.org/10.1016/j.apsusc.2006.12.001.

Geng, Shaoning, Jiang, Ping, Shao, Xinyu, Guo, Lingyu, Gao, Xuesong, 2020. Heat transfer and fluid flow and their effects on the solidification microstructure in full-penetration laser welding of aluminum sheet. J. Mater. Sci. Technol. 46 (11), 50–63. https://doi.org/10.1016/j.jmst.2019.10.027.

Gonzalez, R., Ashrafizadeh, H., Lopera, A., Mertiny, P., Mcdonald, A., 2016. A review of thermal spray metallization of polymer-based structures. J. Therm. Spray Technol. 25 (5), 897–919. https://doi.org/10.1007/s11666-016-0415-7.

Gusarov, A.V., Kruth, J.P., 2005. Modelling of radiation transfer in metallic powders at laser treatment. Int. J. Heat Mass Trans. 48, 3423–3434. https://doi.org/10.1016/j.ijheatmasstransfer.2005.01.044.

Hino, T., Tamura, M., Tanaka, Y., Kouno, W., Makino, Y., Kawano, S., Matsunaga, K., 2009. Development of underwater laser cladding and underwater laser seal welding techniques for reactor components. J. Power Energy Syst. 3 (1), 51–59. https://doi.org/10.1299/jpes.3.51.

Joshi, M.C., Rautela, D.S., Chauhan, R., Suyal, S., 2016. Scrutinize research on underwater welding process: a review. J. Mechan. Civil Eng. 13 (5), 74–78. https://doi.org/10.9790/1684-1305067478.

Kwiecień, Janusz, 2018. The effects of atmospheric turbulence on laser beam propagation in a closed space—an analytic and experimental approach. Opt. Commun. 433. https://doi.org/10.1016/j.optcom.2018.09.022.

Li, Jinyi, Li, Hao Nan, Liao, Zhirong, Axinte, Dragos, 2020. Analytical modelling of full single-track profile in wire-fed laser cladding. J. Mater. Process. Technol. https://doi.org/10.1016/j.jmatprotec.2020.116978 (prepublish).

Liu, Y., Li, C., Huang, X., Ma, K., Luo, X., Li, C., 2020. Effect of water environment on particle deposition of underwater cold spray. Appl. Surf. Sci. 506 (December 2019), 144542 https://doi.org/10.1016/j.apsusc.2019.144542.

Moffatt, E.G., Thomas, M.D.A., 2017. Performance of rapid-repair concrete in an aggressive marine environment. Constr. Build. Mater. 132, 478–486. https://doi.org/10.1016/j.conbuildmat.2016.12.004.

Morita, I., Owaki, K., Yamaoka, H., Kim, C.C., 2006. Study of underwater laser welding repair technology. Weld. World 50 (7–8), 37–43. https://doi.org/10.1007/BF03266534.

Reuther, K., Seyring, M., Schmidt, M.A., Rettenmayr, M., 2019. Convectionless directional solidification in an extremely confined sample geometry. Materialia 8 (June), 100457. https://doi.org/10.1016/j.mtla.2019.100457.

Rowe, M., Liu, S., 2001. Recent developments in underwater wet welding. Sci. Technol. Weld. Join. 6 (6), 387–396. https://doi.org/10.1179/stw.2001.6.6.387.

Seok, B., Lee, N., Thota, S., Gemming, T., Hee, H., 2019. Effects of radiative local heating on metal solidification during selective laser melting for additive manufacturing. Appl. Surf. Sci. 496 (July), 143594 https://doi.org/10.1016/j.apsusc.2019.143594.

Song, Y.S., Li, Y.S., Zhao, G.F., 2004. Factors affecting corrosion and approaches for improving durability of ocean reinforced concrete structures. Ocean. Eng. 31, 779–789. https://doi.org/10.1016/j.oceaneng.2003.07.006.

Song, Boxue, Yu, Tianbiao, Jiang, Xingyu, Xi, Wenchao, Lin, Xiaoli, 2021. Development mechanism and solidification morphology of molten pool generated by laser cladding. Int. J. Therm. Sci. 159. https://doi.org/10.1016/j.ijthermalsci.2020.106579.

Tamanna, N., Crouch, R., Naher, S., 2019. Progress in numerical simulation of the laser cladding process. Opt. Lasers Eng. 122 (May), 151–163. https://doi.org/10.1016/j.optlaseng.2019.05.026.

Tan, Hua, Hu, Tengteng, Wang, Yongxia, Zhang, Fengying, Qiu, Ying, Liu, Tong, Fan, Wei, Zhang, Lai-Chang, 2020. Solidification effect on the microstructure and mechanism of laser-solid-forming-produced flame-resistant Ti–35V–15Cr alloy. Adv. Eng. Mater. 22 (7) https://doi.org/10.1002/adem.202000102.

Wang, X.C., Laoui, T., Bonse, J., Kruth, J.P., Lauwers, B., Froyen, L., 2002. Direct selective laser sintering of hard metal powders: experimental study and simulation. Int. J. Adv. Manuf. Technol. 19, 351–357. https://doi.org/10.1007/s001700200024.

Wang, J., Sun, Q., Pan, Z., Yang, J., Feng, J., 2019. Effects of welding speed on bubble dynamics and process stability in mechanical constraint-assisted underwater wet welding of steel sheets. J. Mater. Process. Tech. 264 (September 2018), 389–401. https://doi.org/10.1016/j.jmatprotec.2018.09.022.

Wei, Ya, Pathiraj, B., Liu, Shaojie, 2016. 2D modelling of clad geometry and resulting thermal cycles during laser cladding. J. Mater. Process. Tech. 230. https://doi.org/10.1016/j.jmatprotec.2020.116978.

Yan, M., Peng, Q., Yin, Q., 2012. Study on stress corrosion crack of austenitic stainless steel in simulated ocean environment. Procedia Eng. 27 (2011), 1538–1543. https://doi.org/10.1016/j.proeng.2011.12.618.

Zuo, P., Chen, S., Wei, M., Liang, J., Liu, C., Wang, M., 2019. Thermal behavior and grain evolution of 24CrNiMoY alloy steel prepared by pre-laid laser cladding technology. Opt. Laser Technol. 119 (April), 105613 https://doi.org/10.1016/j.optlastec.2019.105613.